Stochastic variability of velocity estimates using eikonal tomography on the Long Beach data set

Taylor Dahlke, Gregory Beroza, Jason Chang, Stanford University; Sjoerd de Ridder, University of Science and Technology of China (USTC)*

SUMMARY

One approach to describe the properties of a complex earth system is to use stochastic methods to characterize statistical variability of seismic velocity (Mai and Beroza (2002)). A stochastic modeling approach requires input in the distributions of the model parameters of interest. A spatial field of distributions for each model point describes the spatial variation of velocity. In this work, we use cross-correlations from a Long Beach region data set of ambient seismic noise recordings to perform eikonal tomography for phase velocity. We use Delaunay triangles as our basis for discretizing the model and represent the velocity model as a distribution for each triangle. We take advantage of the fact that our data provides extensive numbers of correlations for each receiver to build histogram distributions of phase velocity for each triangle. These distributions can be integrated with other models to help make inferences about the nature of the geology and tectonics of the region. Besides forming an input to stochastic modeling, these distributions can be used to generate maps of average velocity. Our map of average velocities clearly shows fault lines that are known to traverse the survey.

INTRODUCTION

Dataset overview

The Long Beach 3D seismic array was deployed in two phases by NodalSeismic. Because the array is located in an urban environment it is difficult and disruptive to collect active seismic data. This provides an incentive to attempt exploration approaches that make use of ambient seismic noise. During both surveys, data was recorded 24 hours/day with a sampling rate of 500 Hz. Phase one was recorded from January to June 2011, and phase two from January to April 2012.

For this study we have the last two weeks of recordings available from phase one, and five weeks from phase two. The datasets we used consist of roughly 2500 vertical-component geophones for phase one, and roughly 2400 geophones for phase two (see Figure 1). The coverage areas of these two surveys are adjacent to each other, and overlap slightly. Phase one extends about 9.0 km north-south, and 6.0 km east-west, with the Port of Long Beach being an approximate boundary on the southwestern corner. Phase two is directly east, and is approximately 8.5 km north-south by 4.0 km east-west. Average station spacing is 100 m in phase two, while our phase one data has lower sampling density, since it was collected towards the end of the survey when many geophones were being brought off-line. During acquisition a 3.0 Hz low cut recording filter was applied for both survey phases; however, we were able to recover the suppressed energy in frequencies below 3.0 Hz.

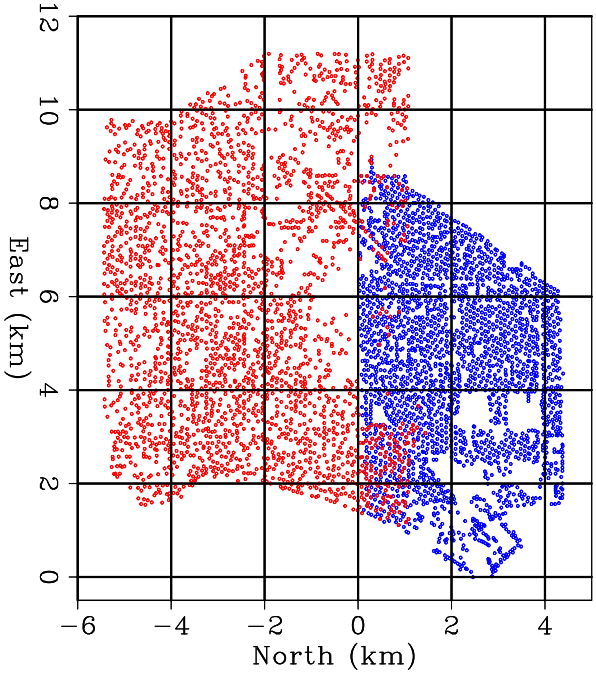

Figure 1: Map of stations in Long Beach survey area. Phase one shown in red, phase two in blue.

Eikonal tomography

Eikonal tomography is based on the principle of taking the magnitude of the spatial derivative of a map of arrival-time values, and then calculating the inverse to get a velocity value. This principle is expressed by the scalar eikonal equation as described in Lin et al. (2009):

$$|\nabla t_i(x)| = c_i^{-1}(x). \tag{1}$$

i indicates the virtual source used to get the time delay value t_i located at position x, while c_i is the velocity value that is calculated. In this work, the spatial domain was discretized as a field of Delaunay triangles between stations. Planar traveltime surfaces were fit in each triangle, and the velocity estimate was computed using the dip of the plane.

Delaunay triangulation

Delaunay triangulation, named for the work of Boris Delaunay (1934), is a triangulation for a set of points such that no point lies inside any triangle. Two aspects of this method are attractive to us.

The first is the simplicity of discretizing with triangles in general. The fewest points necessary to define a plane (or a spatial gradient in both x and y) is three. This simplifies eikonal

DOI http://dx.doi.org/10.1190/segam2014-1541.1

tomography to an analytic expression for the velocity value of each triangle (each triangle being a traveltime surface). The inverse of a spatial gradient calculation for a traveltime surface is a velocity value valid for the center of the triangle. We effectively interpolate this measurement by assigning the velocity value to the entire area within the bounds of the triangle. As a result, this approach defines the eikonal tomography phase velocity at a resolution that is justified by the spatial density of the data sampling.

The second favorable aspect of discretizing with Delaunay triangles is a characteristic of the triangles that this method produces. There are multiple approaches to dividing up a spatial domain of scattered sampling points, but the Delaunay method guarantees that the minimum angle within each triangle is the maximum that is possible from all point combinations. This means the Delaunay discretization minimizes the occurrence of narrow or "skinny" triangles. Very narrow triangles are less reliable interpolators for the three points that they include because the sensitivity of the velocity result is heavily weighted to only one vertex of the triangle. Conversely, triangles that are approximately equilateral have more evenly distributed sensitivity to time delay errors.

WORKFLOW

The inputs to our workflow are the traces derived from cross-correlation as described in Chang et al. (2014). Before cross-correlation the raw traces were whitened, and after cross-correlation the output was normalized. These correlations were performed on two hour time windows for 35 days worth of noise recording. In order to make virtual seismic sources located at each station in the array, we stacked the correlation outputs over time.

Most of the energy in the virtual seismic sources was generated by ocean wave noise from the coastline and travels south-to-north Chang et al. (2013). As a result the virtual seismic sources are not symmetric in time. Assuming reciprocity, we fold the energy from the negative time lags into the positive timelags and sum. This greatly mitigates the directionality in the radiation patterns of the virtual seismic sources. Next, we use a tapered window to isolate the wave train and suppress background correlation fluctuations. The moveout velocity of the tapered window is determined by sorting the traces in radial offset and identifying an average moveout. The taper is then applied on each source-receiver pair with a moveout depending on the particular offset. We next perform the fast Fourier transform (FFT) along the time axis to get the phase information from each trace. We correct the phase of the Fourier domain signal by adding $\frac{\pi}{4}$, according to the far field complex exponential approximation of the Hankel function. Then we filter out traces with "bad" phase values. These "bad" traces included those with extremely high or low values (loud and quiet/dead receivers), as well as those with non-zero phase value at zero frequency. For phase one, about 2% of all traces were discarded on these criteria, with about 4.5% discarded from phase two. Next, we compute the instantaneous phase, and unwrap the phase. We use the relationship between phase

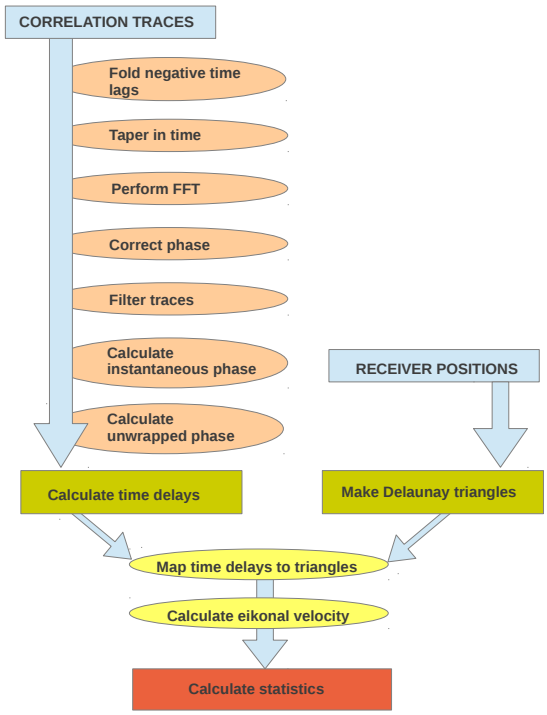

Figure 2: Workflow used to process cross-correlations.

and time delay for a single propagating wave:

$$t_i = \frac{\Theta_i}{2\pi f_i}. \tag{2}$$

With the time delay values calculated for each trace, the next step is to create the Delaunay triangles. Once these are constructed, the time delay values are mapped onto the Delaunay triangles. On this Delaunay mesh, we can calculate the eikonal tomography phase velocities. This results in a histogram for each triangle in the mesh built with velocity estimates from each source (see Figure 3 for an example). Figure 2 outlines the workflow.

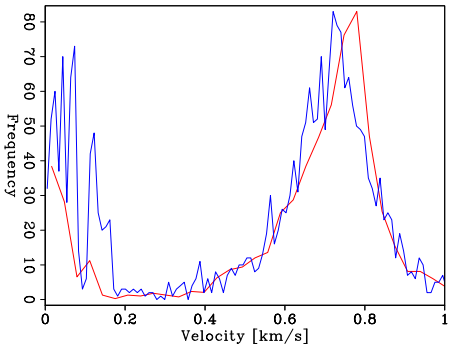

Figure 3: Examples of distributions of wavespeed for 1.0 Hz (red) and 1.25 Hz (blue) for a single triangle.

DOI http://dx.doi.org/10.1190/segam2014-1541.1

The resulting histograms are statistical characterizations of the spatial velocity distributions. There are several ways to draw velocity maps from this statistical characterization. One way may be to find an average velocity for each triangle, or a Moran statistic describing spatial correlation. If the original dataset was associated with a single time interval, then the work flow can be repeated for other time intervals in order to build up a velocity distribution for each triangle. This procedure allows us to form distributions dependent on virtual source position and maintain the direction of wave propagation as a free variable. We could find wave-propagation direction dependent on spatial distribution of velocity and characterize anisotropy. For the results shown here, the velocity values in our distributions varied by virtual source, not by time period (because we have already stacked all time periods beforehand to improve the quality of the virtual seismic sources).

FREQUENCY - WAVENUMBER PLOTS

The frequency-wavenumber plot in Figure 4 was made by sorting the traces from a single virtual source by radial offset, and then performing a two dimensional Fourier transformation. These plots show two streaks of energy projecting from zero frequency, and indicate that two wave modes exist in the correlated data. Furthermore, there are distinct bands of energy that exist at 1.5 Hz, as well as at about 0.1 Hz. The sources of this energy is not apparent at this time. One theory is that this energy is sourced from the below-grade Alameda corridor, which experiences heavy freight rail traffic from the Port of Long Beach.

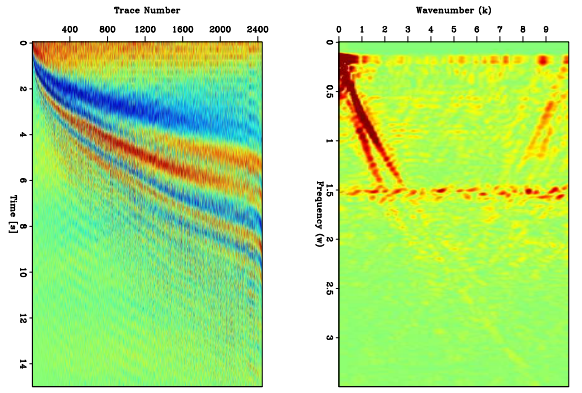

Figure 4: Energy folded into positive lags with traces sorted by radial offset (left). Corresponding f-k plot showing background noise bands and dual surface wave modes (right).

The modes propagate with different velocities, however at small offsets the two modes mix. For this reason, when we calculate the average wavespeeds from each virtual source (at both 1.0 and 1.25 Hz), we exclude those receivers within that offset range (approx 1-2 km). Figure 5 demonstrates this offset zone where mixing occurs for a virtual shot on the eastern part of the phase two survey. When these modes mix, the unwrapped phase values become distorted, and the time delay / velocity values suffer as a result.

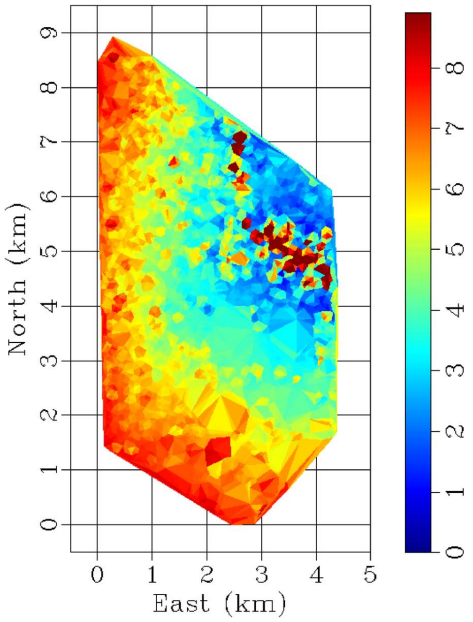

Figure 5: Time delay values for a single virtual shot in the phase two array. Note the triangles in the 1-2 km offset range are corrupted by what appears to be mode mixing. Virtual source is in upper right corner of array.

Excluding these offsets has two effects on the robustness of our statistics. Although we have an effect of increased robustness by excluding erroneous values, by excluding certain offset ranges from our statistics, we also reduce the number of values being summed (the “fold”) for certain areas of the array. For example, we find that by removing the offsets in the range of 1.0 - 2.0 km, we end up reducing the fold value for average velocity measurements in the middle of the phase two array (see Figure 6). Smaller velocity estimate sets can decrease the quality of the statistical description of the spatial velocity distribution.

DISCUSSION

Theoretically, the best results that we should expect for average velocity would be from the super-stack data sets (made by stacking correlations from all time periods), since we would expect the signal-to-noise ratio to be maximized. We run the super-stack correlation traces through our workflow to generate the velocity maps shown in Figure 7. When we look at the average velocity results at 1.0 and 1.25 Hz, we are encouraged to see similarities with the results previously generated by Lin et al. (2013), including the presence of velocity anomalies that seem to indicate the Newport-Inglewood fault.

Conventional ray-tomography is usually regularized forcing smooth maps. Traditional eikonal tomography (Lin et al., 2009) relies on regularization of traveltime measurements to a regular grid. In this step, noise in the traveltime picks is propagated nonlinearly into the regularized traveltime surface. Or alterna-

DOI http://dx.doi.org/10.1190/segam2014-1541.1

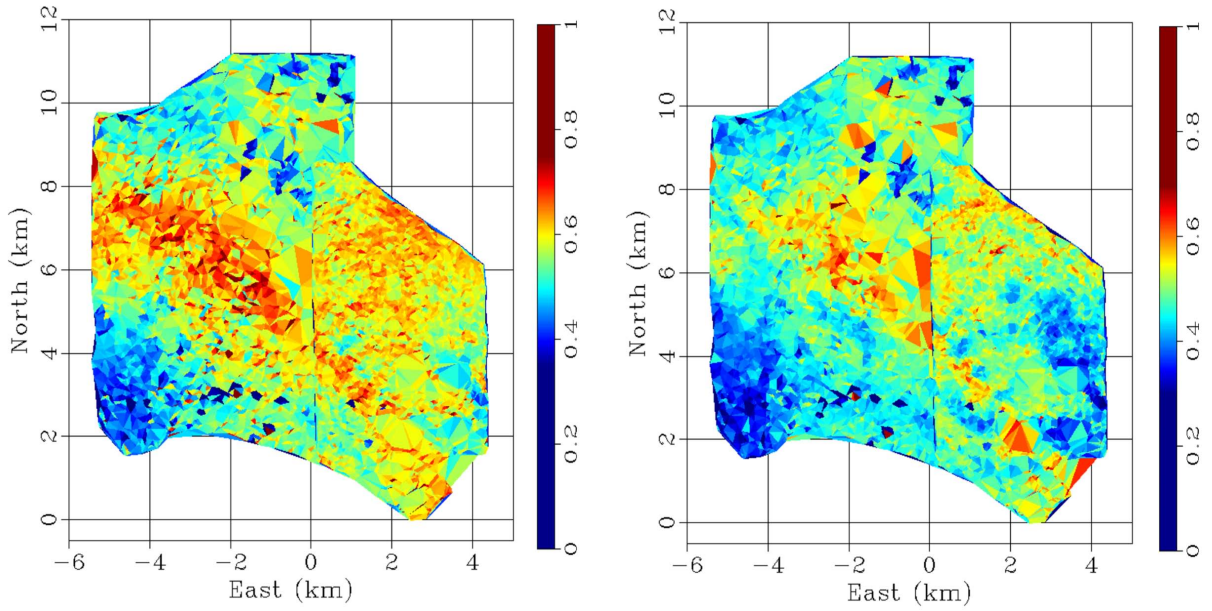

Figure 7: Average wave speed for both phase one and two at 1.0 Hz (left panel) and 1.25 Hz (right panel). Scaling of velocity is in km/s.

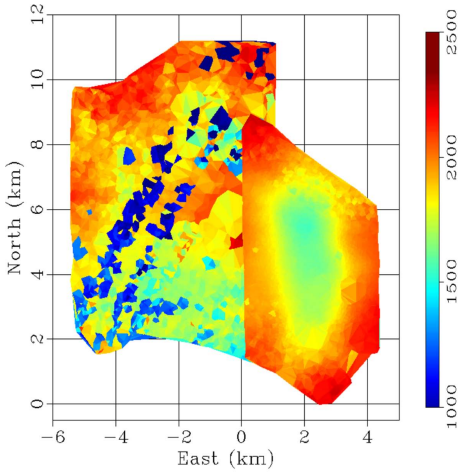

Figure 6: Full array fold map based on 1.0 Hz frequency subset of velocity calculations.

tively, the regularization smooths the traveltimes surface by not fitting the traveltime picks exactly (Mordret et al., 2013). In the method presented here, we bypass the regularization step and find distributions of velocities for each triangle. Generating a smooth velocity map, given the distribution for velocities in each triangle, can be achieved by Kriging with a certain (possibly spatially variable) covariance.

CONCLUSION

Using ambient seismic noise recordings, we use cross-correlations to get phase information, and ultimately derive Rayleigh wave phase velocity estimates for each unit in our triangulation of the spatial domain. From the distributions that are formed using this workflow we can derive statistics, including the average velocity, which we demonstrate here. We found that our results seem to show the same fault lines that we know to cross the surveys. Future work includes refining the statistical robustness of our velocity estimates, as well calculating statistics related to spatial correlation length so that characteristics of the larger region can be inferred.

ACKNOWLEDGMENTS

I would like to thank Sjoerd de Ridder, Greg Beroza and Biondo Biondi for their advising guidance and insight to this work. I would also like to thank Signal Hill Petroleum and NodalSeismic for providing us with the Long Beach dataset. Lastly, I would like to thank the sponsors of SEP for their generous support.

DOI http://dx.doi.org/10.1190/segam2014-1541.1

http://dx.doi.org/10.1190/segam2014-1541.1

EDITED REFERENCES

Note: This reference list is a copy-edited version of the reference list submitted by the author. Reference lists for the 2014 SEG Technical Program Expanded Abstracts have been copy edited so that references provided with the online metadata for each paper will achieve a high degree of linking to cited sources that appear on the Web.

REFERENCES

Chang, J. P., R. Clapp, N. Nakata, B. Biondi, and S. de Rid-der, 2014, High-frequency surface and body waves from ambient noise crosscorrelations at Long Beach, CA: Presented at the 84th Annual International Meeting, SEG.

Chang, J. P., S. de Ridder, and B. Biondi, 2013, Power spectral densities and ambient noise crosscorrelations at Long Beach: Presented at the 83rd Annual International Meeting, SEG.

Delaunay, B., 1934, Sur la sphère vide a la moire de georges vorono?: Bulletin de l'Acadamie des Sciences de l'URSS: Classe des sciences math matiques et na, **6**, 793–800.

Lin, F.-C., D. Li, R. W. Clayton, and D. Hollis, 2013, High-resolution 3D shallow crustal structure in Long Beach, California: Application of ambient noise tomography on a dense seismic array: Geophysics, **78**, no. 4, Q45–Q56, http://dx.doi.org/10.1190/geo2012-0453.1.

Lin, F. C., M. H. Ritzwoller, and R. Snieder, 2009, Eikonal tomography: Surface wave tomography by phase front tracking across a regional broadband seismic array: Geophysical Journal International, **177**, no. 3, 1091–1110, http://dx.doi.org/10.1111/j.1365-246X.2009.04105.x.

Mai, P. M. and G. C. Beroza, 2002, A spatial random field model to characterize complexity in earthquake slip: Jour nal of Geophysical Research: Solid Earth, **107**, ESE 10–1–ESE 10–21.

Mordret, A., N. Shapiro, S. Singh, P. Roux, and O. I. Barkved, 2013, Helmholtz tomography of ambient noise surface wave data to estimate Scholte wave phase velocity at Valhall Life of the Field: Geophysics, **78**, no. 2, WA99–WA109, http://dx.doi.org/10.1190/geo2012-0303.1.